Electronic Supplementary Material (ESI) for Inorganic Chemistry Frontiers.

Supporting Information

Water-stable halide coordination polymer with dual self-trapped exciton emission for dual-mode Hg^{2+} sensing

Yin-Jing Shi,‡ Xianghua Yang,‡ Hou-Rong He, Wei-Ming Liao,* Hua-Qun Zhou, Lai-Hon Chung, Lin Yu and Jun He*

Experimental Section

DFT calculation

All calculations were performed with periodic DFT using the Gaussian plane wave method implemented in CP2K's Quickstep module.[1,2] The explorative studies of the catalysts structure were performed using the molecularly optimized basis set DZVP-MOLOPT-SR-GTH for each atom with a Goedecker-Teter-Hutter (GTH) pseudopotential.[3-6] The calculations were conducted using the generalized gradient approximation and the Perdew-Burke-Ernzerhof (PBE) functional[7] for DOS and Band Structure. A 2D **XCP-1** was employed and 2 × 2 × 1 supercell with 572 atoms model was employed to calculated DOS and Band Structure. The k-path of Band Structure was generated by SeeK-path,[8] insert 10 point in every path. An energy convergence for the self-consistent field (SCF) calculation was set to 2×10^{-6} Hartree. The energy cutoff of 400 Ry was used throughout the calculations.

The excited state structure was optimized by TDDFPT with Auxiliary Density Matrix Method (ADMM) approximated PBE functional and semiempirical Simplified Tamm−Dancoff Approximation (sTDA) in the CP2K program package.[9-11] The ADMM basis cFIT3 has been used for C, H, O, S element and admm-dzp has been used for Pb and I. The Convergence criterion of all excitation energies was set as 1×10^{-7} eV.

All the input file was generated by Multiwfn.[12] The structure and VBM/CBM pictures were generated by VESTA.[13]

Supporting figures and tables

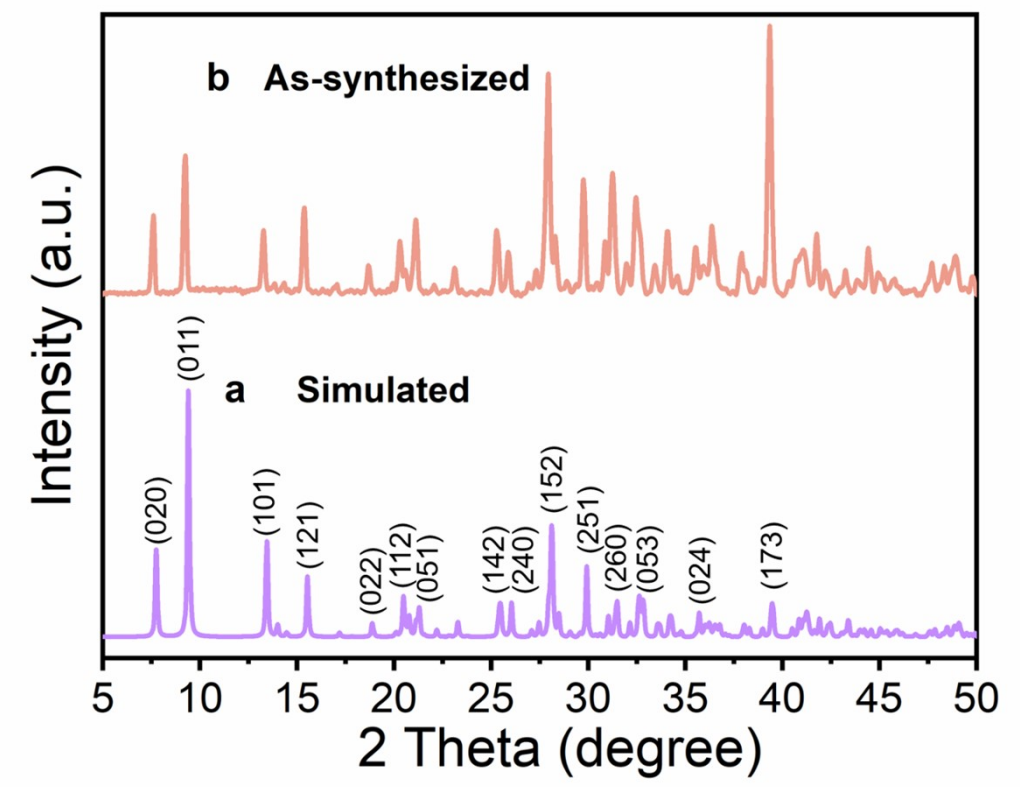

Figure S1. PXRD patterns of (a) simulated and (b) as-synthesized **XCP-1**.

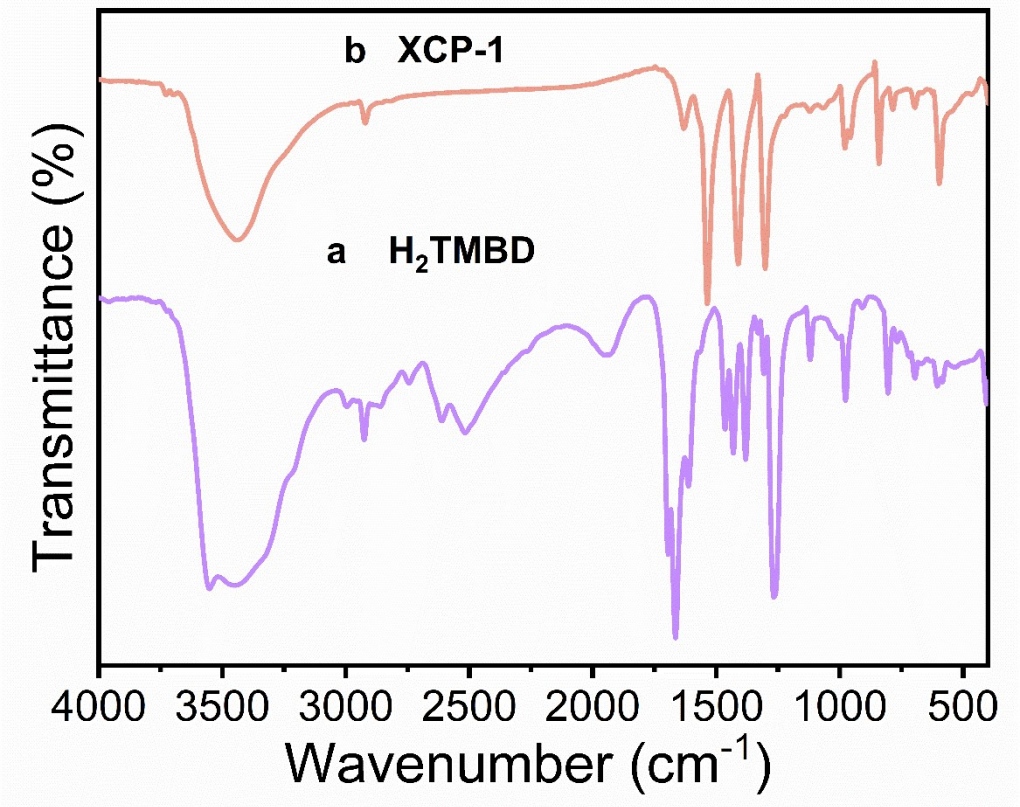

Figure S2. FT-IR spectra of (a) the ligand H_2TMBD and (b) as-synthesized **XCP-1**.

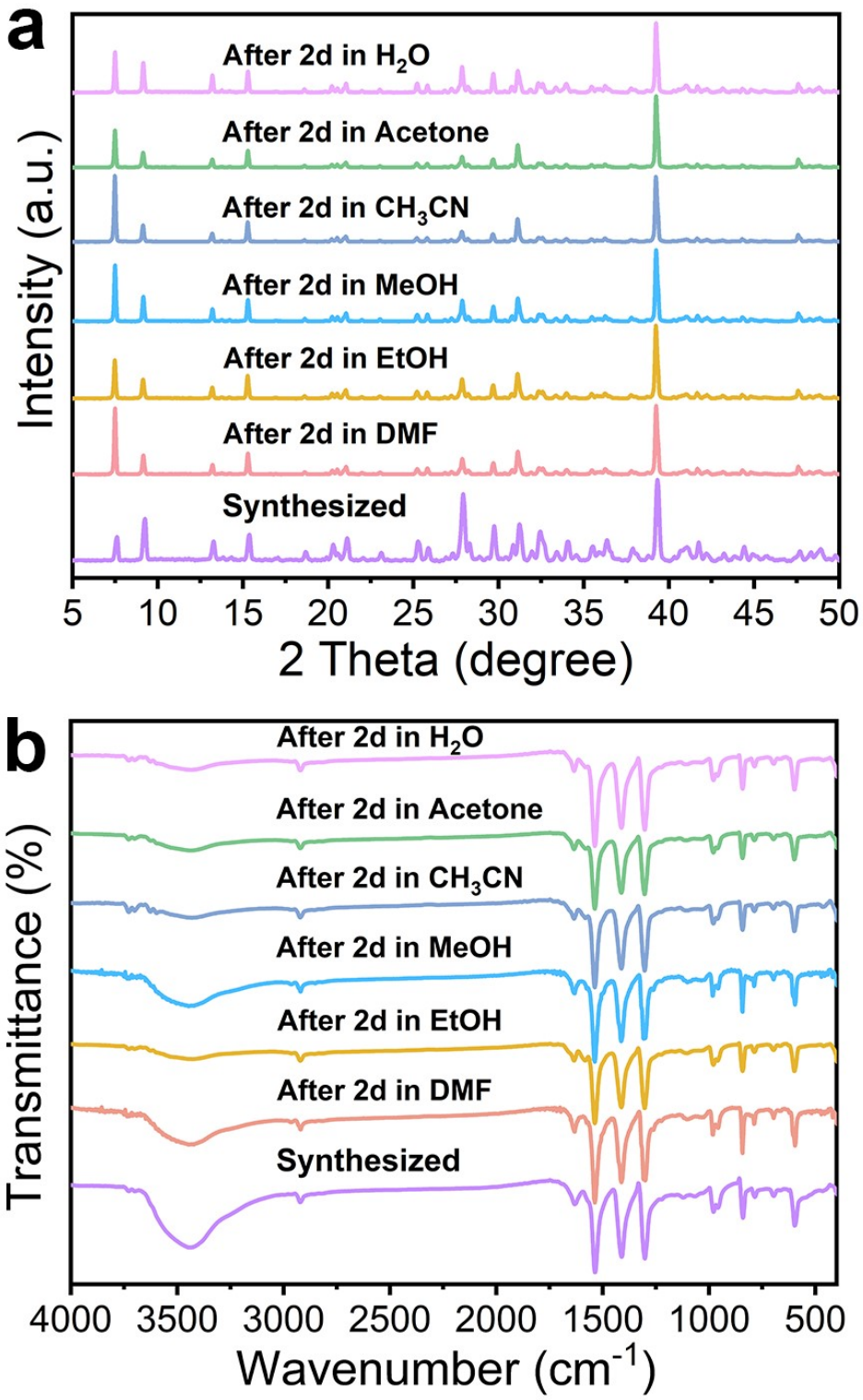

Figure S3. (a) PXRD patterns and (b) FT-IR spectra of **XCP-1** before and after treatment in different solvents for 48 h.

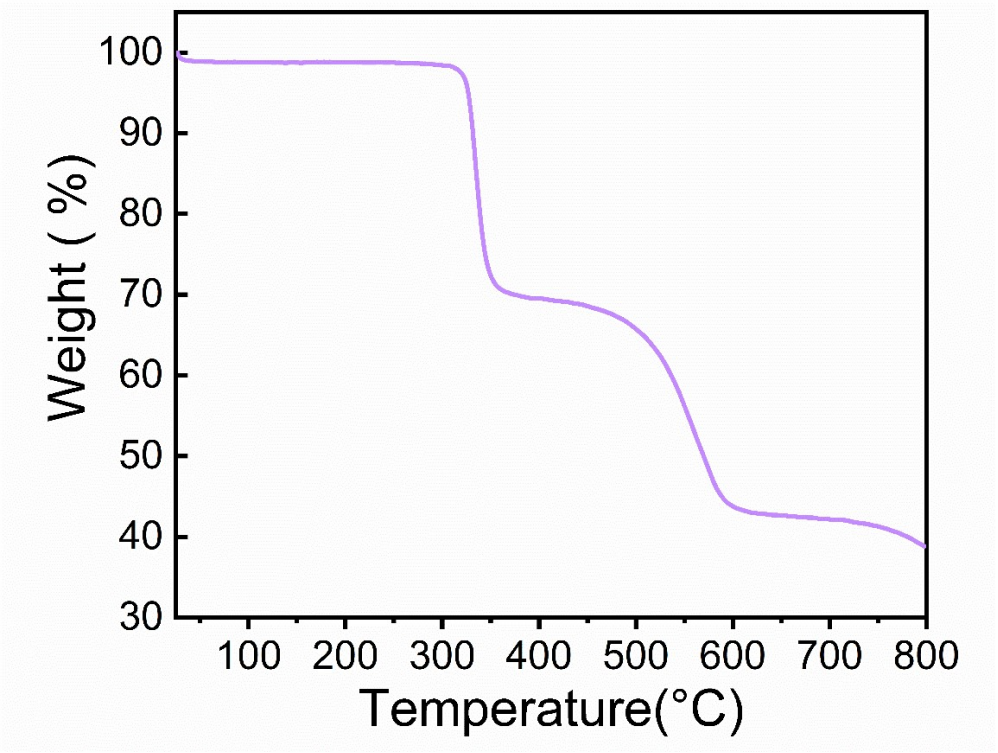

Figure S4. Thermogravimetric curve of **XCP-1** under N_2 atmosphere.

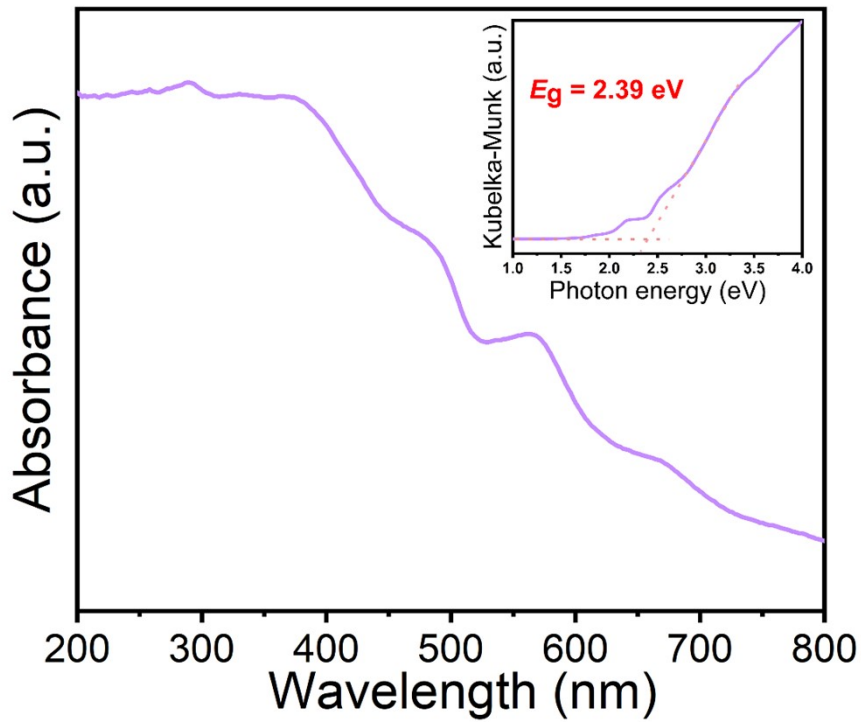

Figure S5. Absorption spectrum of **XCP-1** by UV-vis diffuse reflectance measurement. Inset: Kubelka–Munk plot transformed from diffuse reflectance data.

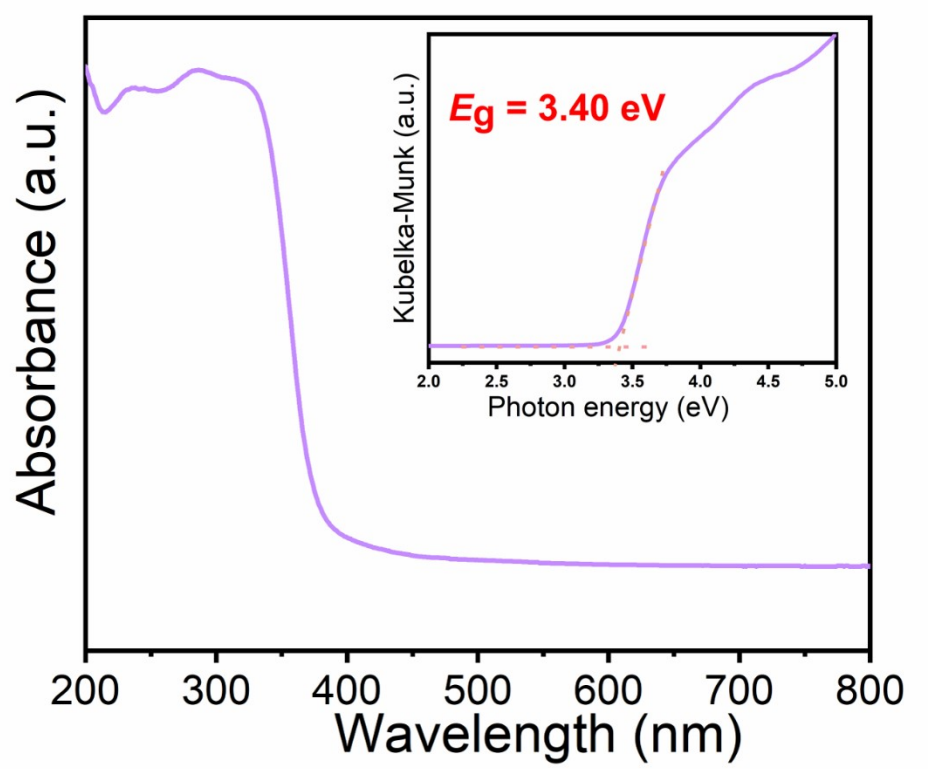

Figure S6. Absorption spectrum of H_2TMBD by UV-vis diffuse reflectance measurement. Inset: Kubelka–Munk plot transformed from diffuse reflectance data.

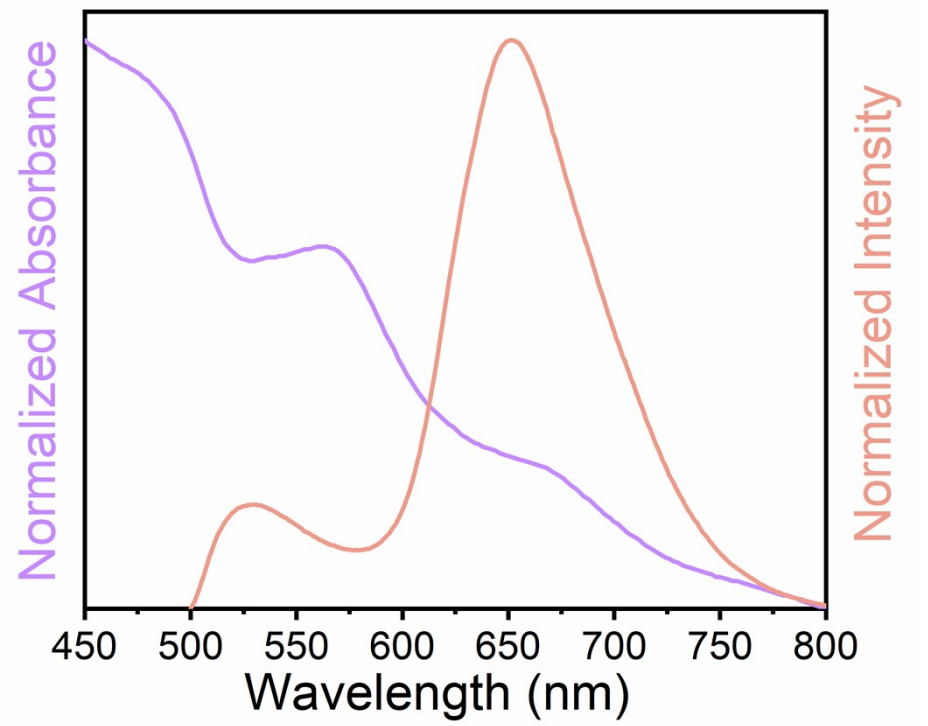

Figure S7. The absorption and emission (λ_{ex}= 450 nm) spectra of **XCP-1**.

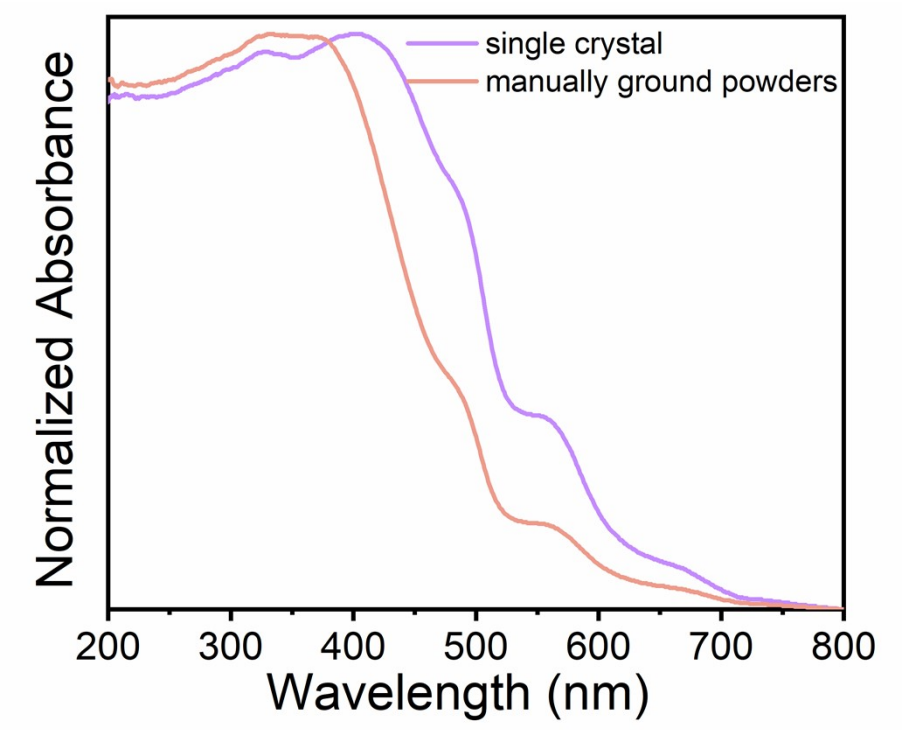

Figure S8. UV-vis absorption spectra of **XCP-1** in single-crystal state and manually ground powders.

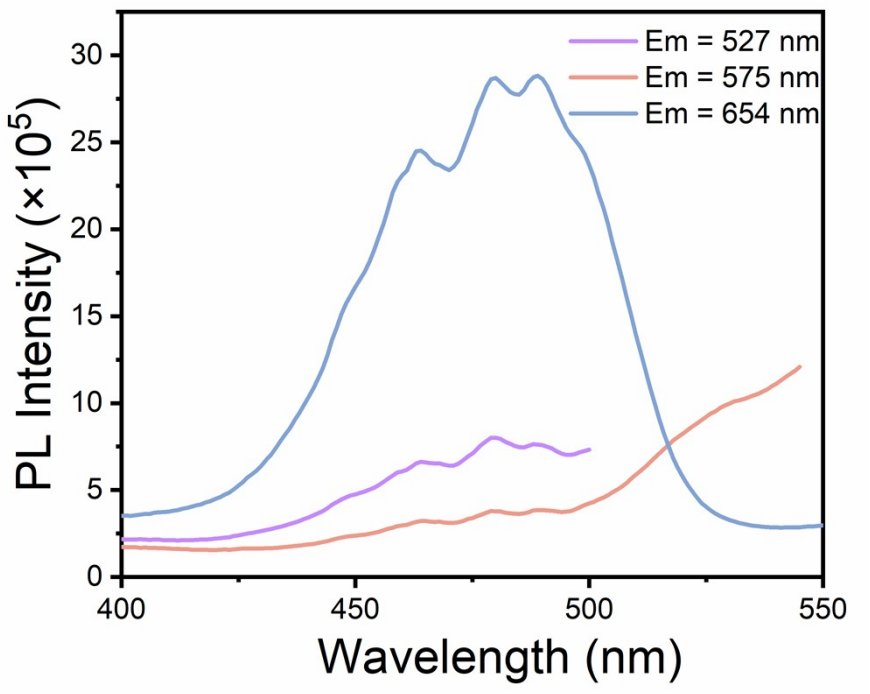

Figure S9. Excitation spectra of **XCP-1** when monitored by 527, 575 and 654 nm.

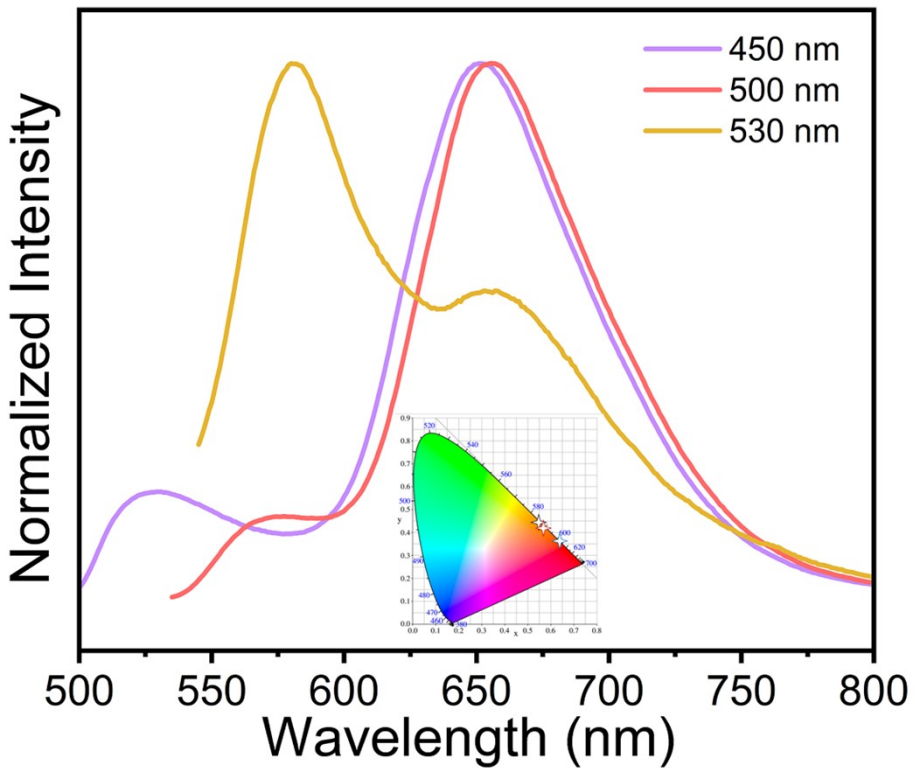

Figure S10. Photoluminescent spectra and CIE coordinate diagrams of **XCP-1** under excitation at 450, 500, and 530 nm, respectively.

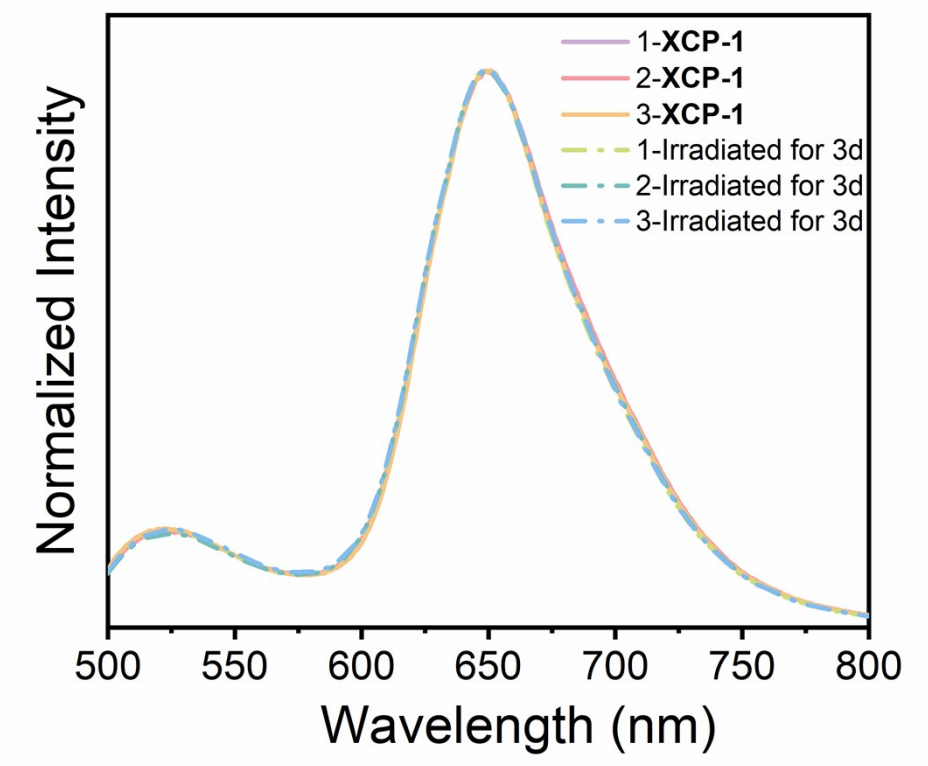

Figure S11. Emission spectra of three sample of **XCP-1** measured after irradiation for 3d.

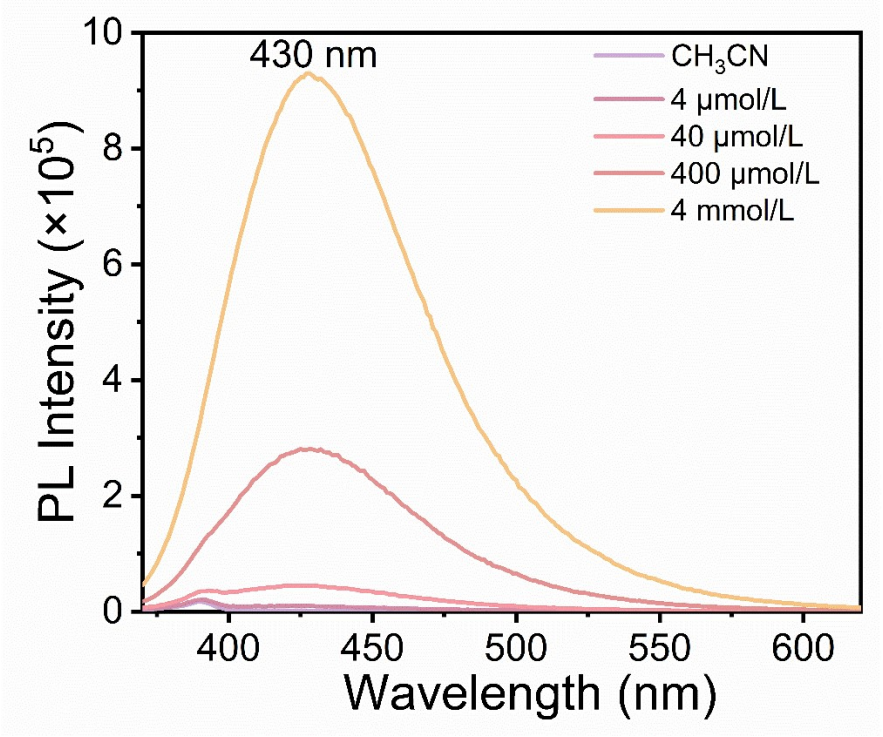

Figure S12. The emission spectra of H_2TMBD at different concentrations when excited at 350 nm.

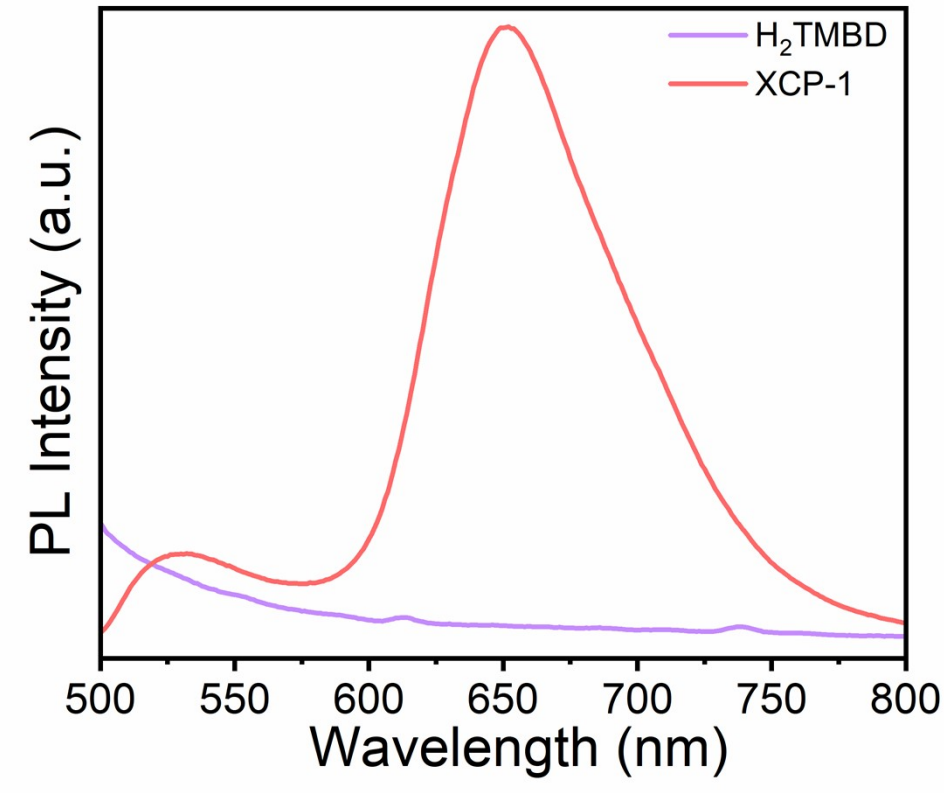

Figure S13. The emission spectra of **XCP-1** and ligand H_2TMBD when excited at 450 nm.

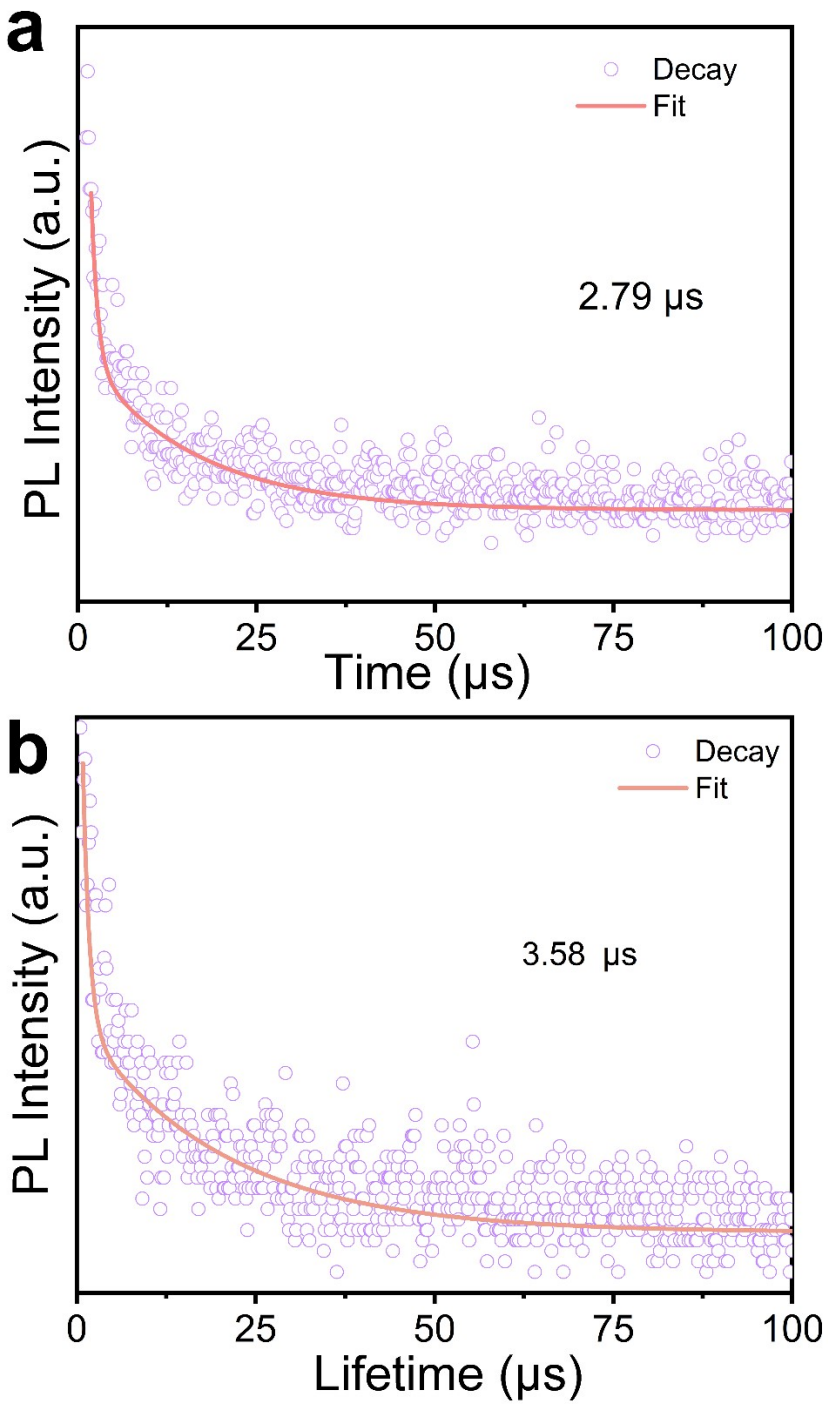

Figure S14. Photoluminescent decay curve and fitting plot of **XCP-1** for the emission peak at 527 nm at (a) 300 K and (b) 78 K, respectively when excited at 450 nm.

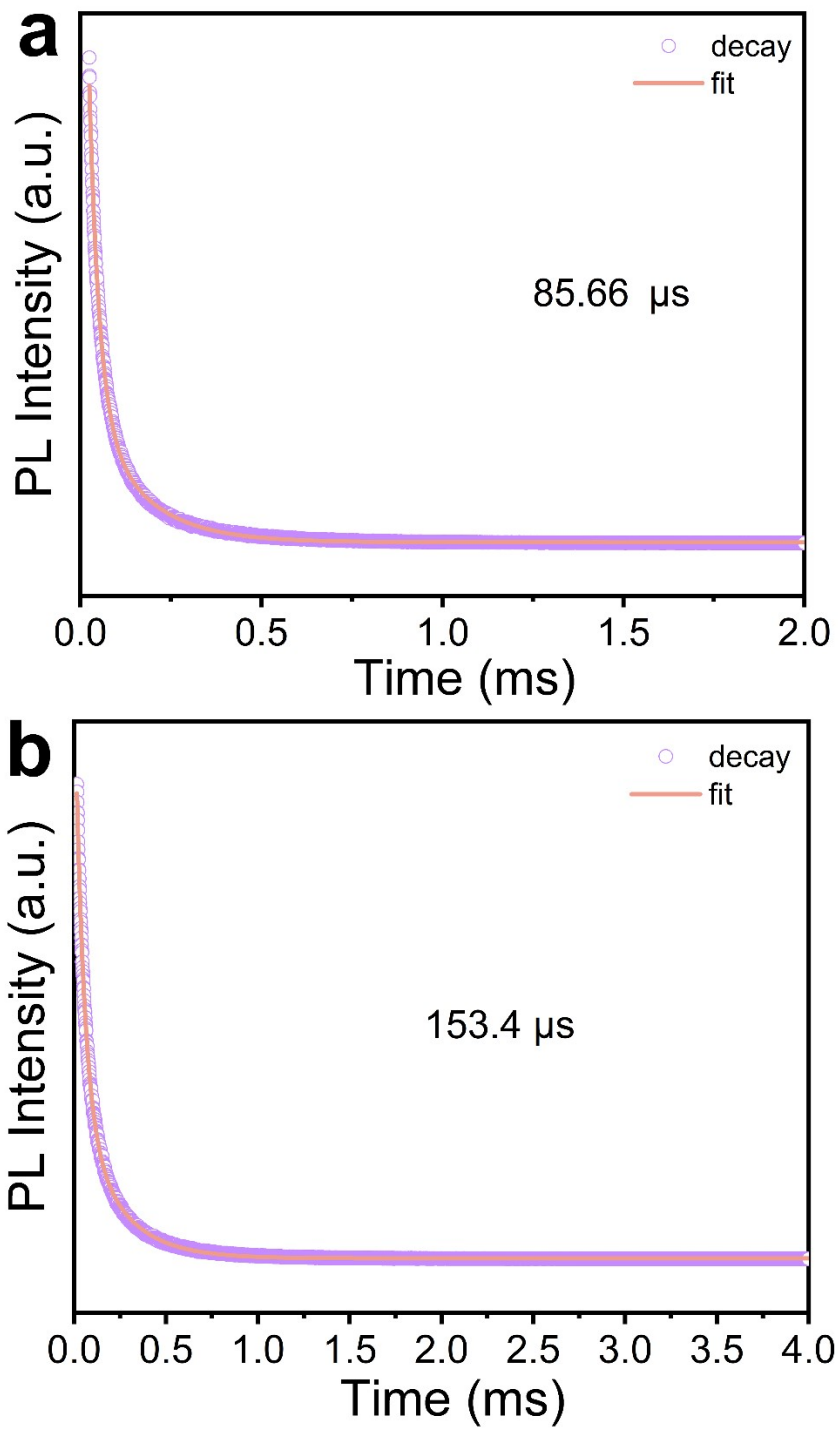
a
decay
fit
85.66 μs
PL Intensity (a.u.)
0.0
0.5
1.0
1.5
2.0
Time (ms)
b
decay
fit
153.4 μs
PL Intensity (a.u.)
0.0
0.5
1.0
1.5
2.0
2.5
3.0
3.5
4.0
Time (ms)

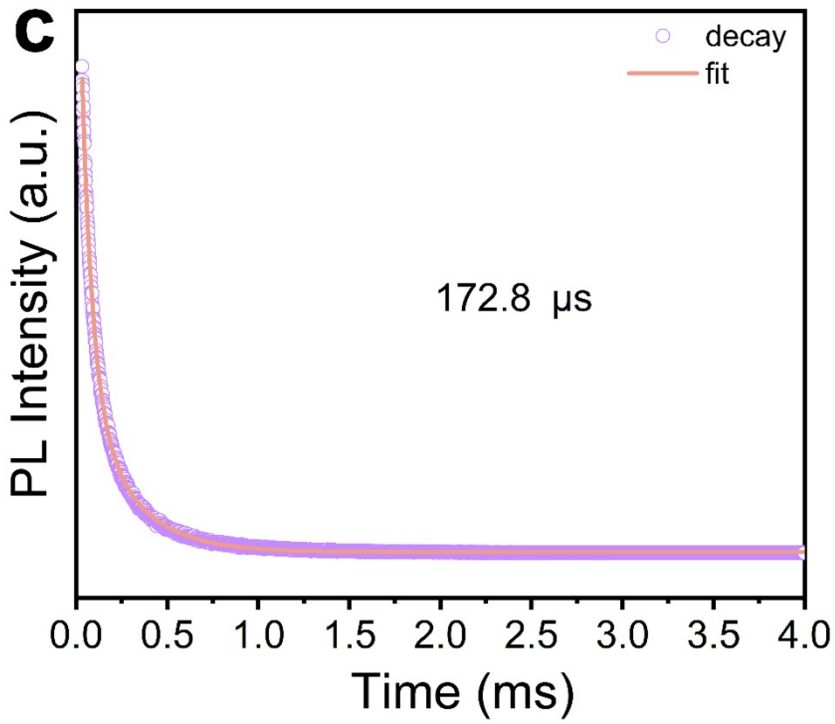

Figure S15. Photoluminescent decay curve and fitting plot of **XCP-1** for the emission peak at 654 nm at (a) 300 K, (b) 200 K and (c) 78 K, respectively when excited at 450 nm.

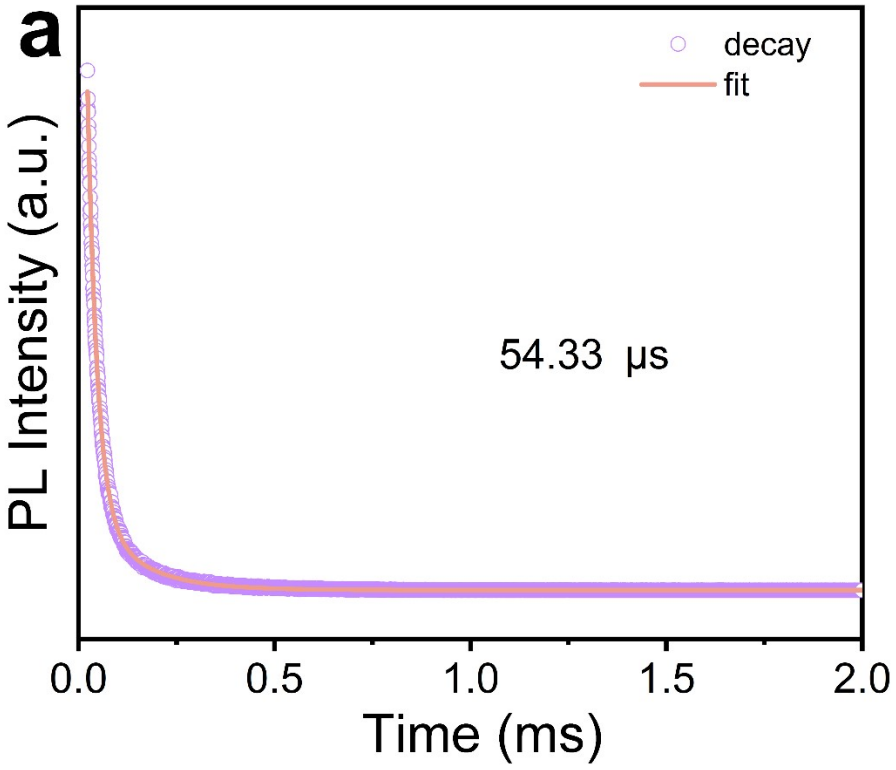

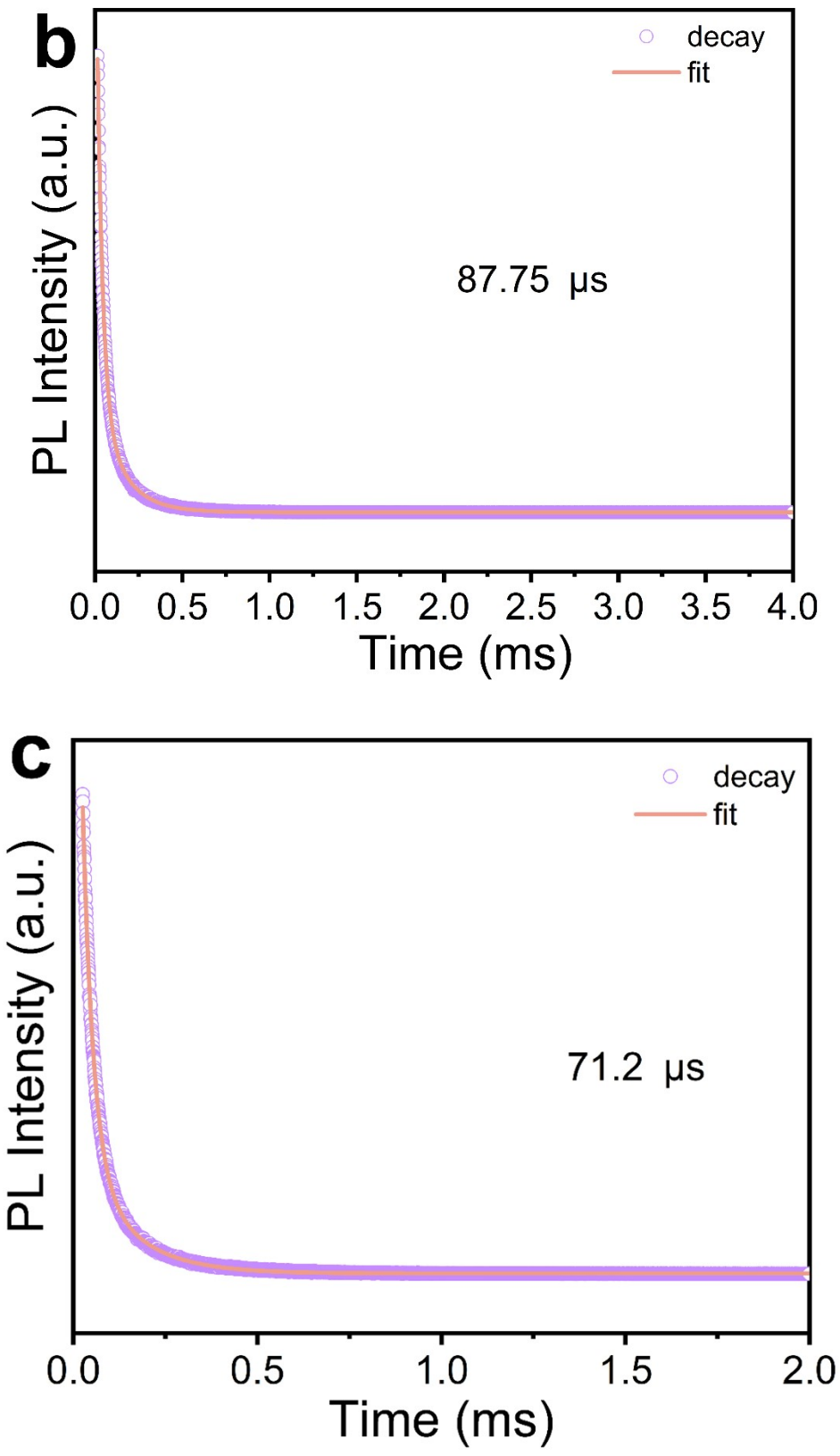

Figure S16. Photoluminescent decay curve and fiting plot of **XCP-1** for the emission peak at 654 nm at (a) 78 K, (b) 200 K and (c)300 K, respectively when excited at 510 nm.

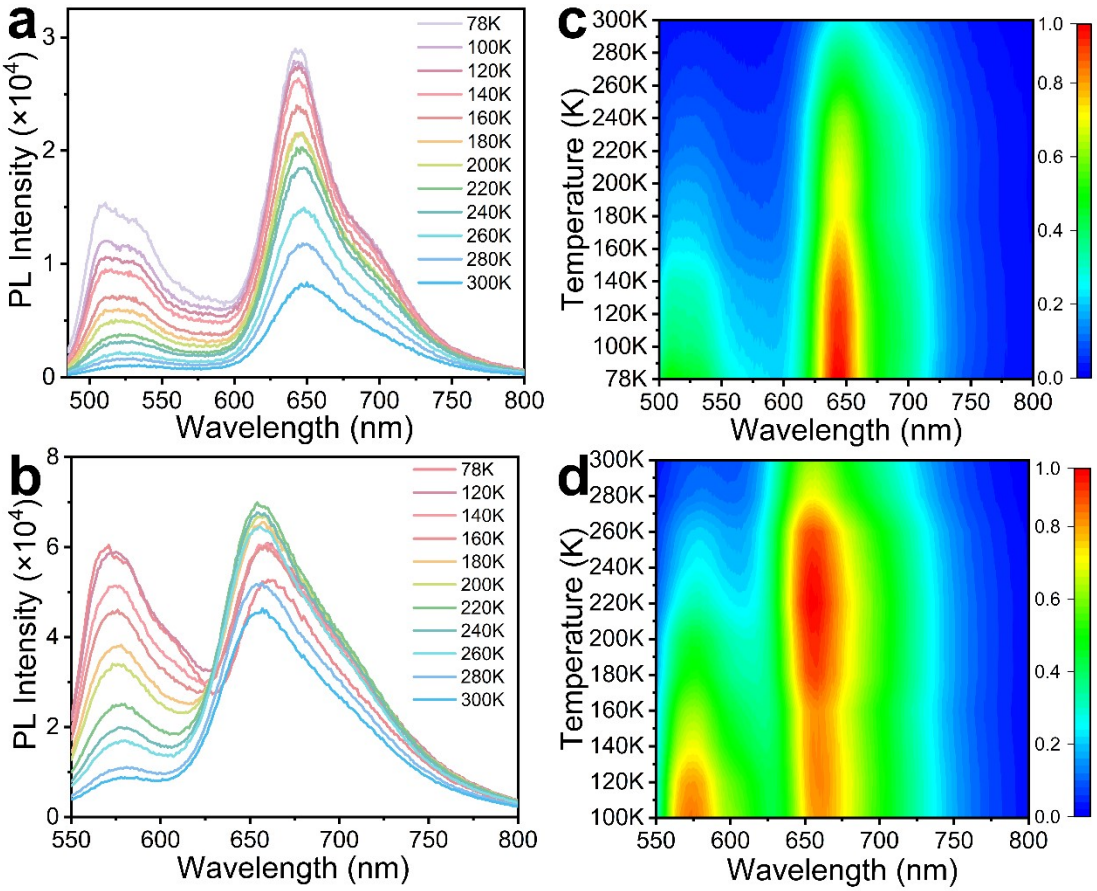

Figure S17. (a, b) Temperature-dependent emission spectra and (c, d) photoluminescent correlation maps of **XCP-1** with excitation wavelength at (a, c) 450 and (b, d) 510 nm, respectively.

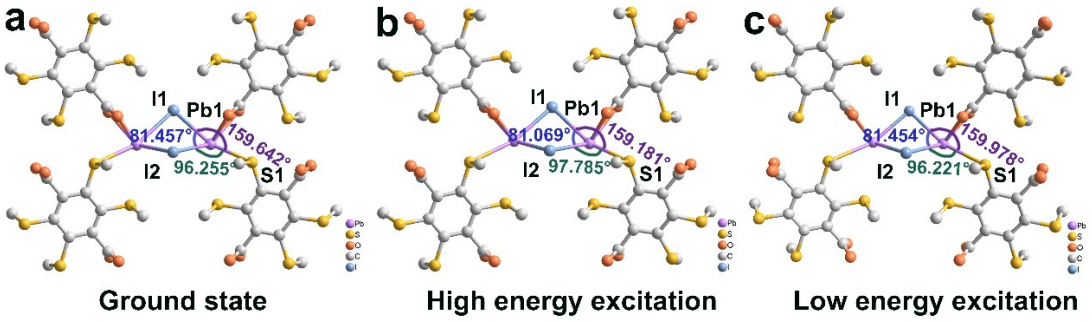

Figure S18. Deformed structures of ground state and excited states of **XCP-1** upon different excitation energy calculating from DFT method.

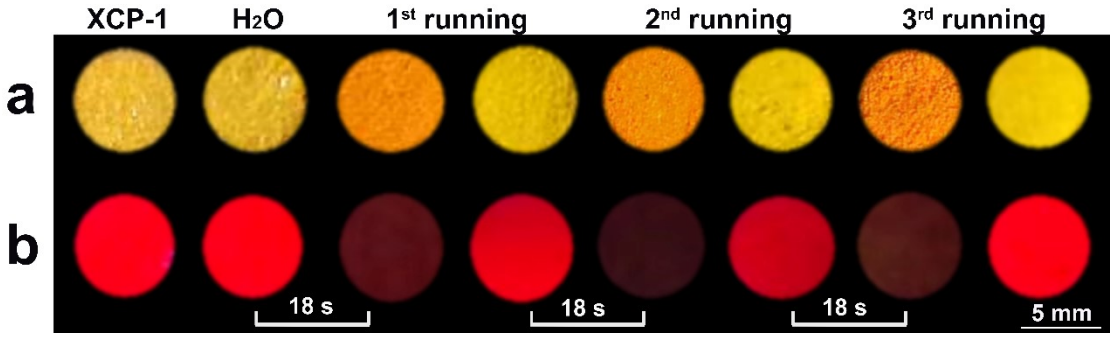

Figure S19. The photographs under (a) ambient light and (b) UV 360 nm of **XCP-1** obtained from the cycling experiments of immersion in 700 ppm Hg^{2+} solution for 18 s or successively washing with ethanol.

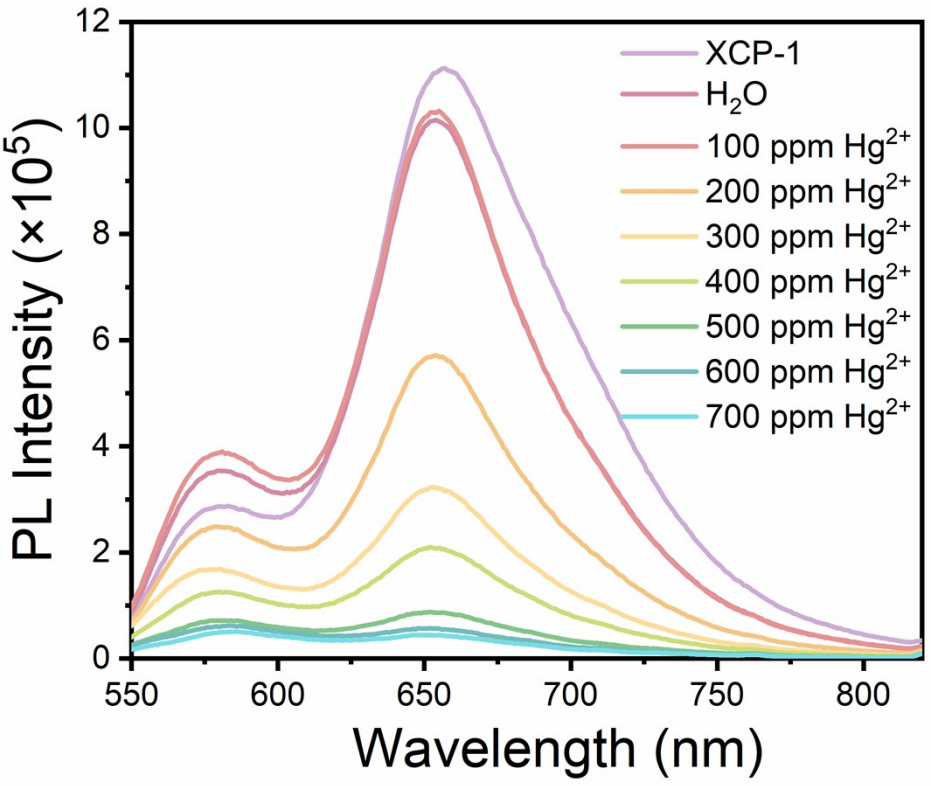

Figure S20. Photoluminescent spectra of **XCP-1** after immersion in Hg^{2+} solutions with different concentrations when excited at 510 nm.

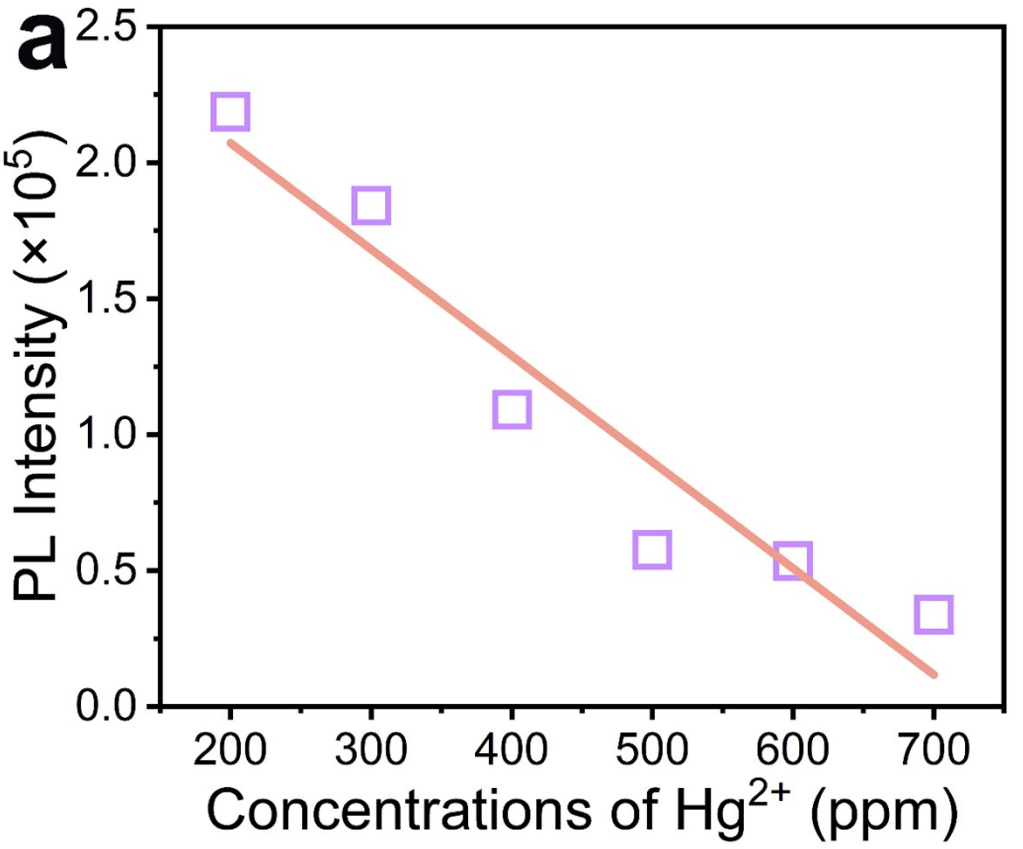
a
PL Intensity (×10^5)
2.5
2.0
1.5
1.0
0.5
0.0
200
300
400
500
600
700
Concentrations of Hg2+ (ppm)

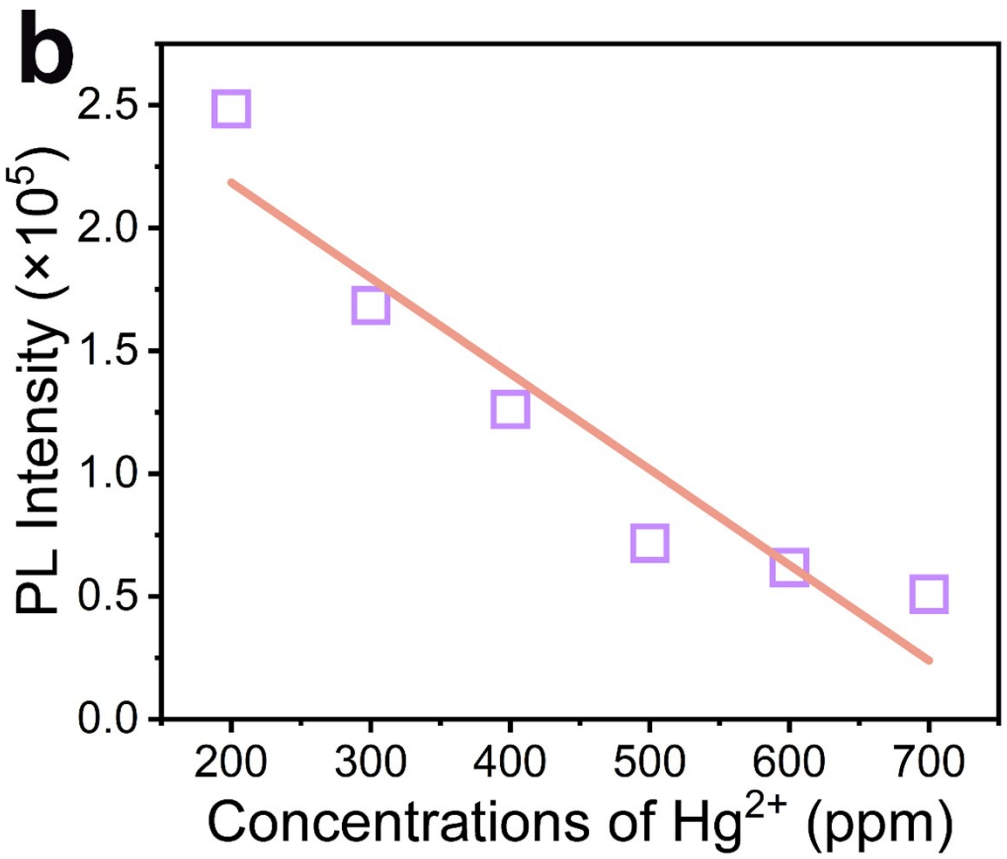
b
PL Intensity (×10^5)
2.5
2.0
1.5
1.0
0.5
0.0
200
300
400
500
600
700
Concentrations of Hg2+ (ppm)

Figure S21. Plots of photoluminescence intensity *vs.* Hg^{2+} concentrations varying from 200 to 700 ppm. (a) Emission intensity at 527 nm when excited at 450 nm (correlation coefficient: 0.920), (b) Emission intensity at 575 nm when excited at 510 nm (correlation coefficient: 0.902), and (c) Emission intensity at 654 nm when excited at 510 nm (correlation coefficient: 0.864).

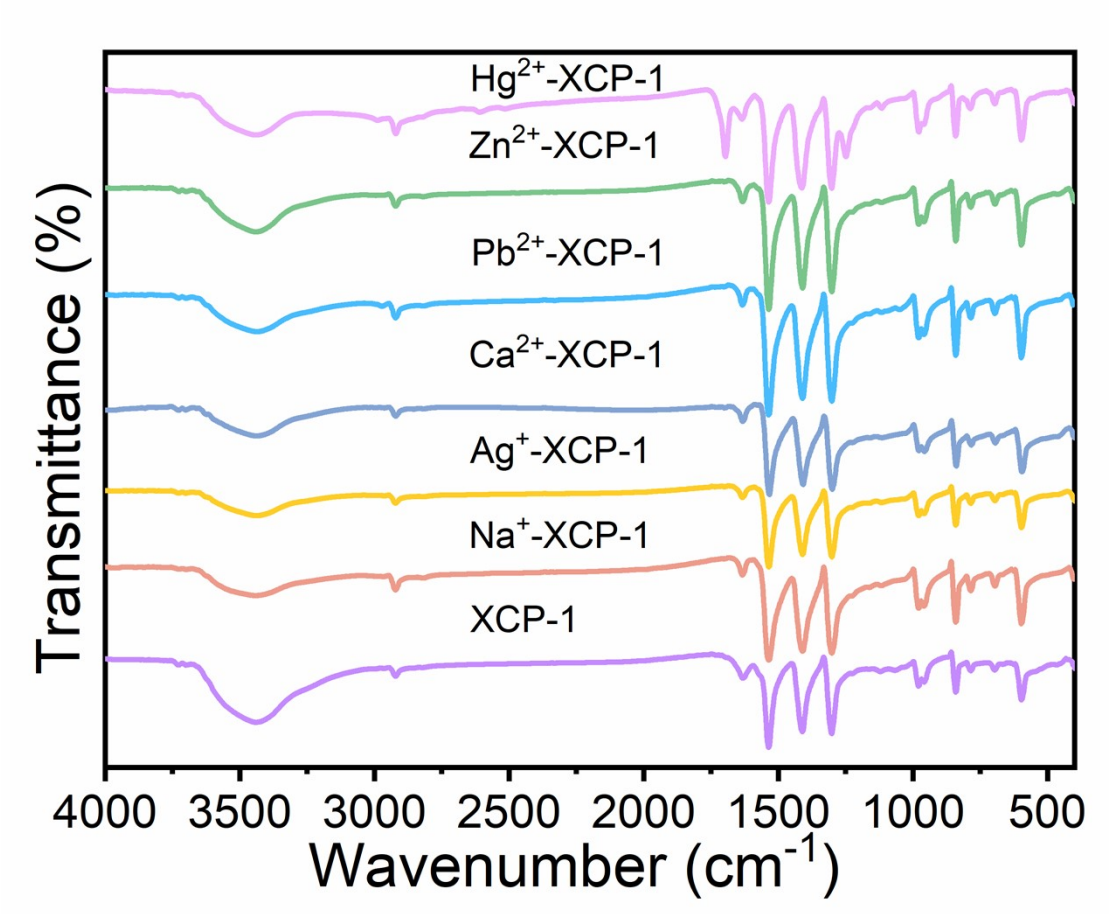

Figure S22. The FT-IR spectra of **XCP-1** after immersion in different metal ion solutions.

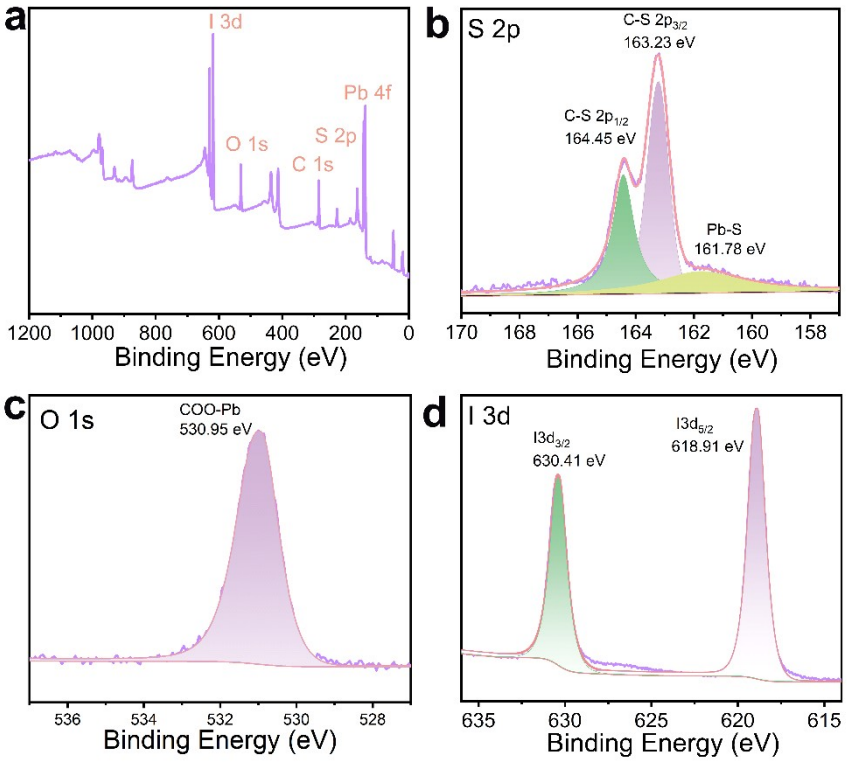

Figure S23. (a) XPS spectra of **XCP-1**. High-resolution (b) S 2p, (c) O 1s, and (d) I 3d spectrum.

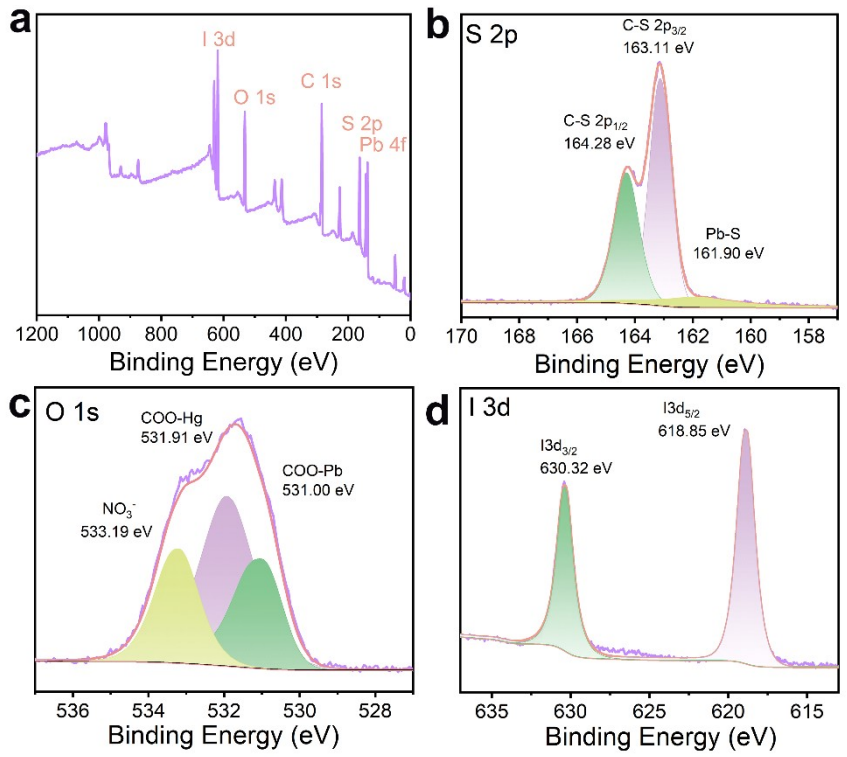

Figure S24. (a) XPS spectra of **XCP-1** after treatment in 700 ppm Hg^{2+} solution. High-

resolution (b) S 2p, (c) O 1s, and (d) I 3d spectrum.

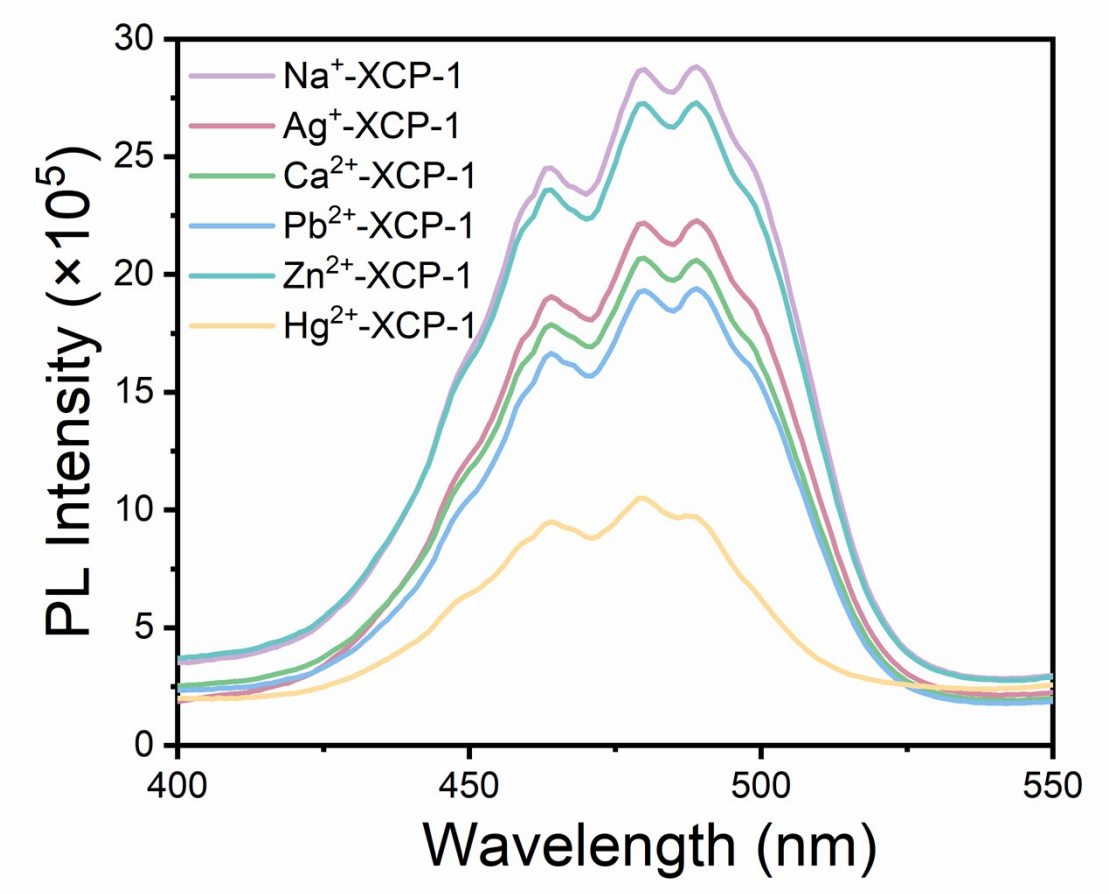

Figure S25. The excitation spectra of **XCP-1** after immersion in different metal ion solutions.

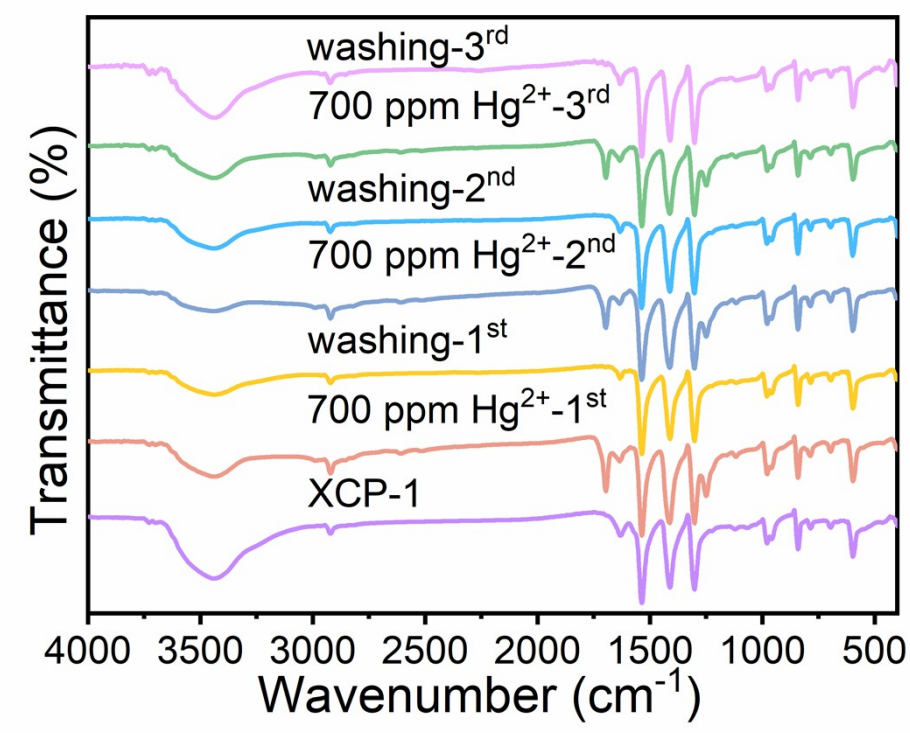

Figure S26. FT-IR spectra of **XCP-1** obtained from the cycling experiments of immersion in 700 ppm Hg^{2+} solution for 18 s or successively washing with ethanol.

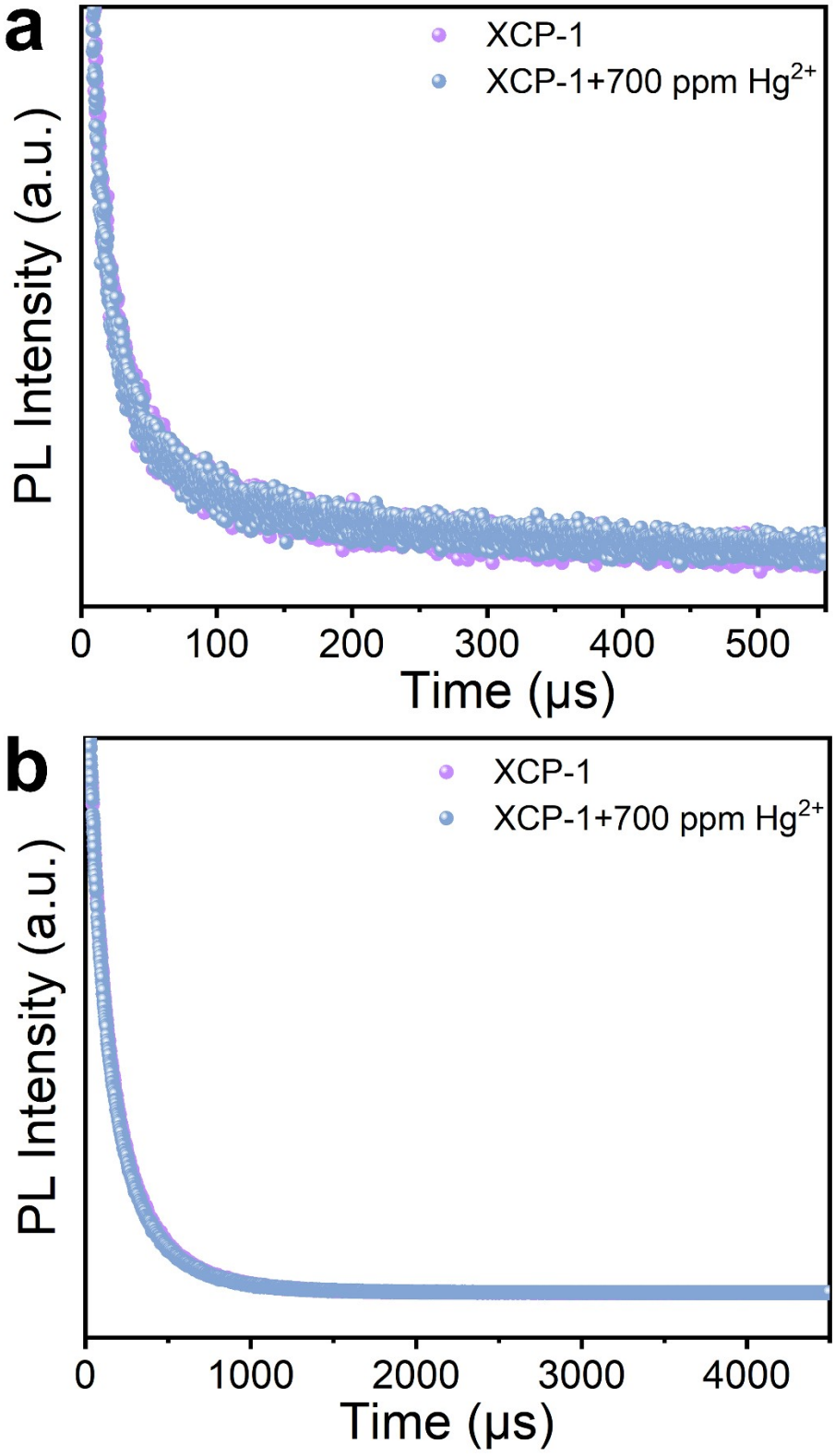

Figure S27. Photoluminescent decay curve of **XCP-1** and **XCP-1**+700 ppm Hg^{2+} for the emission peak at (a) 527 nm and (b) 654 nm, respectively when excited at 359 nm.

Table S1. Crystallographic data and structure refinement result for **XCP-1.**

Compound	**XCP-1**
Empirical formula	$C_6H_6IO_2PbS_2$
Formula weight	508.32
Temperature (K)	300 K
Crystal system	orthorhombic
Space group	*Pnma*
Unit cell dimensions	*a* (Å)=8.5418(7) *b* (Å)=22.790(2) *c* (Å)= 10.2937(10) *α* (°)= 90 *β* (°)= 90 *γ* (°)= 90
V(Å^3), Z	2003.9(3), 8
Density (calculated) (g cm^{-3})	3.370
F(000)	1800.0
Goodness-of-fit on F^2	1.042
Final R indexes [I>=2σ (I)]	R_1 = 0.0271, wR_2 = 0.0648
Final R indexes [all data]	R_1 = 0.0303, wR_2 = 0.0667

$R_1=\sum(||F_0|-|F_c||)/\sum|F_0|$; [b] $wR_2=(\sum w(F_0^2-F_c^2)^2/\sum w(F_0^2)^2)^{1/2}$

Table S2. Summary of luminescent lifetimes for **XCP-1**.

Temperature [K]	**λ_{ex} [nm]**	**λ_{em} [nm]**	**τ_{av} [µs]**
300	450	527	2.79
78	450	527	3.58
300	450	654	85.66
200	450	654	153.4
78	450	654	172.8
300	510	654	71.2
200	510	654	87.75
78	510	654	54.33

Table S3. Summary of photophysical properties for **XCP-1** at 300 and 77 K.

Temperature [K]	λ_{em} [nm]	Stokes Shift [nm (eV)]	FWHM [nm]
300	527[a]	77 (0.40)	116
78	527[a]	77	72
300	654[a]	204 (0.86)	73
78	654[a]	204	58
300	575[b]	125 (0.27)	125
78	575[b]	125	70
300	654[b]	204 (0.54)	80
78	654[b]	204	83

[a] and [b] represents the excitation wavelength is 450 and 510 nm, respectively.

References

1. Kuhne, T. D. et al. CP2K: An electronic structure and molecular dynamics software package - Quickstep: Efficient and accurate electronic structure calculations. *J. Chem. Phys.* **152**, 194103 (2020).
2. VandeVondele, J. et al. Quickstep: Fast and accurate density functional calculations using a mixed Gaussian and plane waves approach. *Comput. Phys. Commun.* **167**, 103-128 (2005).
3. Krack, M. Pseudopotentials for H to Kr optimized for gradient-corrected exchange-correlation functionals. *Theor. Chem. Acc.* **114**, 145-152 (2005).
4. VandeVondele, J. & Hutter, J. Gaussian basis sets for accurate calculations on molecular systems in gas and condensed phases. *J. Chem. Phys.* **127** (2007).
5. Lippert, B. G., Parrinello, J. H. & Michele. A hybrid Gaussian and plane wave density functional scheme. *Mol. Phys.* **92**, 477-488 (2010).
6. Hartwigsen, C., Goedecker, S. & Hutter, J. Relativistic separable dual-space Gaussian pseudopotentials from H to Rn. *Phys. Rev. B* **58**, 3641-3662 (1998).
7. Perdew, J. P., Burke, K. & Ernzerhof, M. Generalized Gradient Approximation Made Simple. *Phys. Rev. Lett.* **77**, 3865-3868 (1996).
8. Hinuma, Y., Pizzi, G., Kumagai, Y., Oba, F. & Tanaka, I. Band structure diagram paths based on crystallography. *Comput. Mater. Sci.* **128**, 140-184 (2017).
9. Risthaus, T., Hansen, A. & Grimme, S. Excited states using the simplified Tamm–Dancoff-Approach for range-separated hybrid density functionals: development and application. *Phys. Chem. Chem. Phys.* **16**, 14408-14419 (2014).
10. Hehn, A.-S. et al. Excited-State Properties for Extended Systems: Efficient Hybrid Density Functional Methods. *J. Chem. Theory Comput.* **18**, 4186-4202 (2022).
11. VandeVondele, J. & Hutter, J. An efficient orbital transformation method for electronic structure calculations. *J. Chem. Phys.* **118**, 4365-4369 (2003).
12. Lu, T. & Chen, F. Multiwfn: a multifunctional wavefunction analyzer. *J. Comput. Chem.* **33**, 580-592 (2012).
13. Momma, K. & Izumi, F. VESTA 3for three-dimensional visualization of crystal, volumetric and morphology data. *J. Appl. Crystallogr.* **44**, 1272-1276 (2011).